DOI: 10.1002/ejic.200700854

Synthesis and Crystal Structure of Mercury-Substituted Type-I Clathrates $A_8Hg_4Sn_{42}$ (A = K, Rb, Cs)

Andreas Kaltzoglou,[a] Siméon Ponou,[a] and Thomas F. Fässler*[a]

Keywords: Clathrate / Differential thermal analysis / Mercury / Stannides / Crystal structure / Zintl phases

The mercury-substituted type-I clathrates $A_8Hg_4Sn_{42}$,with A = K, Rb or Cs, were obtained by fusion of the pure elements at high temperatures. The crystal structures of the compounds were refined from single-crystal X-ray diffraction data. They crystallize in the space group $Pm\bar{3}n$ (No. 223), Z = 1 with a = 12.1255(4) Å for $K_8Hg_4Sn_{42}$ (**1**), a = 12.1838(4) Å for $Rb_8Hg_4Sn_{42}$ (**2**) and a = 12.2130(4) Å for $Cs_8Hg_4Sn_{42}$ (**3**). The 3D framework of four-bonded atoms defines two types of polyhedral cages of different size that are fully occupied by the alkali-metal atoms. All three compounds are considered as formally charge-balanced Zintl phases without any homogeneity range. Differential thermal analysis (DTA) indicates that the stability of the clathrates significantly depends on the size of the encaged cations. The thermal stability of the title compounds and the binary phases A_8Sn_{44} (A = K, Rb, Cs) is discussed. Temperature-dependent magnetic measurements for compound **3** show also the expected diamagnetic behaviour.

Introduction

Group-14 clathrates are a distinctive class of high-symmetry inclusion compounds that appear promising for applications such as thermoelectric materials.[1] Their theoretical potential for high thermoelectric efficiency[2] originates from the PGEC (phonon-glass and electron-crystal) concept,[3] according to which a compound can exhibit low lattice thermal conductivity (κ_L) due to the rattling of the encaged metal cations in the rigid four-bonded framework as well as high electrical conductivity due to the delocalised excess electrons in the conduction band. Over the last decade, many reports on the physical properties of clathrates came to forefront, and in contrast to the binary clathrates, some of their ternary analogues, for example, $Sr_8Ga_{16}Ge_{30}$[4] and $Ba_8Ga_{16}Ge_{30}$,[5] can reach relatively high figures of merit (ZT) under ambient conditions. It is now well established that even subtle alternations in the structure or composition of the framework may significantly affect the phonon scattering and ultimately the κ_L of the compounds.[4b,6]

These findings raised interest in the search for reliable ways to synthesise new doped clathrates in high purity and to study their physical properties. In this paper, we report the synthesis, crystal structures, thermal analysis and magnetic properties of the type-I clathrates $K_8Hg_4Sn_{42}$ (**1**), $Rb_8Hg_4Sn_{42}$ (**2**) and $Cs_8Hg_4Sn_{42}$ (**3**), which are substituted by the heavy transition metal Hg.

[a] Technische Universität München, Department Chemie
Lichtenbergstraße 4, 85747 Garching, Germany
Fax: +49-8928913186
E-mail: Thomas.Faessler@lrz.tum.de

Results and Discussion

The title compounds were obtained in high crystallinity and almost as pure phases by high-temperature reactions of stoichiometric mixtures of the elements in niobium ampoules. Some small amounts of the Hg_1Sn_9 alloy[7] were also detected by X-ray powder diffraction. Compounds **1** to **3** adopt the clathrate-I structure (Figure 1) with a primitive cubic cell (space group $Pm\bar{3}n$, Z = 1), and the framework of the Sn atoms is partially substituted by Hg atoms and with alkali metals as guest atoms. The crystallographic sites of the tetrahedrally bonded framework atoms are 6*c*, 16*i* and 24*k*, and those of the (endohedral) guest atoms are 2*a* and 6*d* (Table 1). The Hg atoms have a strict preference for the 6*c* site, which is mixed occupied with Sn1. The total occupancy of these sites is constrained during the structure refinement cycles to unity.

The arrangement of the 46 clathrand atoms in the unit cell defines two types of polyhedra with different sizes: a 20-atom pentagonal dodecahedron [5^{12}], and a 24-atom tetrakaidecahedron [$5^{12}6^2$] (the symbol [$5^{12}6^2$] denotes a polyhedron with 12 pentagonal and 2 hexagonal faces). There are eight cages per formula unit, two small and six large ones, which are occupied by alkali-metal atoms. The tetrakaidecahedra share common hexagonal faces and form nonintersecting "channels" parallel to the three cell axes. The 6*c* sites of such hexagonal faces are distributed along a 4_2 screw axis that runs through the centres of the hexagonal faces and the centres of the polyhedra. As a result, the structure contains no Hg–Hg framework contacts. Possible superstructure reflections indicating lowering of the symmetry due to the ordering of Hg in substituted positions (site 6*c*) were observed neither in powder nor in single-crys-

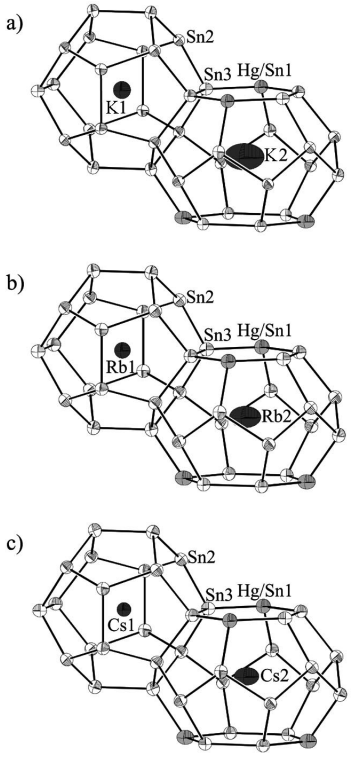

Figure 1. Partial view of the clathrate crystal structures with atom labelling. The alkali-metal, mixed Hg/Sn and Sn positions are drawn as filled grey, filled light grey and white ellipsoids, respectively. All thermal ellipsoids are presented at 90% probability: (a) $K_8Hg_4Sn_{42}$, (b) $Rb_8Hg_4Sn_{42}$ and (c) $Cs_8Hg_4Sn_{42}$. The extent of rattling for the encaged alkali metals in the tetrakaidecahedra follows the order K > Rb > Cs.

Table 1. Atomic coordinates and equivalent isotropic displacement parameters for **1**, **2** and **3**.

Atom	Site	*x*	*y*	*z*	s.o.f.	U_{eq}[a] /Å^2
$K_8Hg_4Sn_{42}$ (**1**)						
K1	2*a*	0	0	0	1	0.027(2)
K2	6*d*	1/4	1/2	0	1	0.118(4)
Hg/Sn1	6*c*	1/2	1/4	0	0.667/0.333	0.0200(3)
Sn2	16*i*	0.18286(3)	*x*	*x*	1	0.0123(3)
Sn3	24*k*	0.31161(4)	0.11758(4)	0	1	0.0136(3)
$Rb_8Hg_4Sn_{42}$ (**2**)						
Rb1	2*a*	0	0	0	1	0.0222(7)
Rb2	6*d*	1/4	1/2	0	1	0.0730(9)
Hg/Sn1	6*c*	1/2	1/4	0	0.667/0.333	0.0215(3)
Sn2	16*i*	0.18309(3)	*x*	*x*	1	0.0148(2)
Sn3	24*k*	0.31132(4)	0.11777(4)	0	1	0.0154(2)
$Cs_8Hg_4Sn_{42}$ (**3**)						
Cs1	2*a*	0	0	0	1	0.0173(4)
Cs2	6*d*	1/4	1/2	0	1	0.0463(4)
Hg/Sn1	6*c*	1/2	1/4	0	0.667/0.333	0.0227(3)
Sn2	16*i*	0.18335(3)	*x*	*x*	1	0.0147(2)
Sn3	24*k*	0.31108(5)	0.11811(5)	0	1	0.0155(2)

[a] U_{eq} is defined as one third of the trace of the orthogonalized U^{ij} tensor.

tal diffraction patterns, even when measured at –140 °C. Note that a corresponding superstructure was recently reported for the binary phases $Rb_8Sn_{44}\square_2$ and $Cs_8Sn_{44}\square_2$ with partially ordered vacancies (□) at 20 °C (space group $Ia\bar{3}d$). At higher temperatures, a higher degree of disorder (space group $Pm\bar{3}n$) by means of an enantiotropic phase transition was observed.[8]

As shown in Table 2, the Sn–Sn bond lengths range from 2.8201(5) to 2.8514(7) Å, from 2.8240(5) to 2.8695(7) Å, and from 2.8198(5) to 2.8850(9) Å in **1**, **2**, and **3**, respectively. The longest distance in all cases is found for the Sn3–Sn3 contact (site 24*k*). Similar Sn–Sn distances were also observed in $Cs_8Zn_4Sn_{42}$ [2.810(4)–2.880(4) Å].[9] In the title compounds, the shortest bond length is observed for Hg/Sn1–Sn3 with 2.7922(3), 2.8072(6), and 2.8139(4) Å for A = K, Rb and Cs, respectively. As a result of the larger atomic size of Hg, a distance increase with respect to homoatomic Sn–Sn contacts is expected. In fact, these distances are found here to be even shorter than the sum of the covalent radii of Sn and Hg (1.40 + 1.50 = 2.90 Å). However, shorter Hg–Sn contacts with respect to normal Sn–Sn contacts are also observed in other intermetallic systems such as BaHgSn[10] [*d*(Hg–Sn) = 2.8068 and 2.8072(3) Å] and also in the molecule $\{MeSi[SiMe_2N(p\text{-Tol})]_3Sn\}_2M$ with M = Zn, Cd, and Hg. In the latter case, the M–Sn bond lengths are crystallographically determined as 2.5782(4), 2.6758(1), and 2.6495(2) Å for Zn, Cd, and Hg, respectively, and the very slight decrease from Cd to Hg is attributed to the relativistic contraction of the 6s valence shell.[11]

More generally, it is expected that the Sn–Sn distances in the framework will increase with the increasing size of the guest metal atoms. All bond lengths but one follow this

Table 2. Interatomic distances for **1**, **2** and **3**.

$K_8Hg_4Sn_{42}$ (**1**) Atomic pairs		*d* /Å	$Rb_8Hg_4Sn_{42}$ (**2**) Atomic pairs		*d* /Å	$Cs_8Hg_4Sn_{42}$ (**3**) Atomic pairs		*d* /Å
Hg/Sn1	–Sn3	2.7922(3) 4×	Hg/Sn1	–Sn3	2.8072(6) 4×	Hg/Sn1	–Sn3	2.8139(4) 4×
Sn2	–Sn2	2.8201(5)	Sn2	–Sn2	2.8240(5)	Sn2	–Sn2	2.8198(5)
	–Sn3	2.8249(6) 3×		–Sn3	2.8373(5) 3×		–Sn3	2.8430(7) 3×
Sn3	–Sn3	2.8514(7)	Sn3	–Sn3	2.8695(7)	Sn3	–Sn3	2.8850(9)
K1	–Sn2	3.8404(4) 8×	Rb1	–Sn2	3.8637(4) 8×	Cs1	–Sn2	3.8785(4) 8×
	–Sn3	4.0385(5) 12×		–Sn3	4.0554(6) 12×		–Sn3	4.0638(6) 12×
K2	–Sn3	4.0546(4) 8×	Rb2	–Sn3	4.0769(5) 8×	Cs2	–Sn3	4.0898(5) 8×
	–Hg/Sn1	4.2870(1) 4×		–Hg/Sn1	4.3076(1) 4×		–Hg/Sn1	4.3179(1) 4×
	–Sn2	4.5130(4) 8×		–Sn2	4.5331(4) 8×		–Sn2	4.5423(4) 8×
	–Sn3	4.6968(2) 4×		–Sn3	4.7166(2) 4×		–Sn3	4.7233(2) 4×

trend; the Sn2–Sn2 length slightly decreases from 2.8240(5) Å in **2** to 2.8198(5) Å in **3**. In all cases, the alkali-metal atoms in the cages are quite distant from the framework atoms and the interaction distances increase with increasing atomic size of the alkali metal. Furthermore, the atomic displacement parameters for the guest alkali metals show almost isotropic behaviour for A1 (2*a* Wyckoff site) in the smaller cavity and anisotropic characteristics for A2 (6*d* Wyckoff site) with U_{11} roughly half the value of U_{22} = U_{33} (Table 3). The ratio U_{22}(A2)/U_{22}(A1) is roughly 5 for the case A = K phase, close to 4 for A = Rb and approximately 3 for A = Cs.

Table 3. Anisotropic displacement parameters for **1**, **2** and **3**.

Atom	U_{11}	U_{22}	U_{33}	U_{12}	U_{13}	U_{23}
$K_8Hg_4Sn_{42}$ (**1**)						
K1	0.027(2)	U_{11}	U_{11}	–	–	–
K2	0.063(5)	0.145(6)	U_{22}	–	–	–
Hg/Sn1	0.0158(3)	0.0285(5)	U_{11}	–	–	–
Sn2	0.0123(3)	U_{11}	U_{11}	–0.0009(1)	U_{12}	U_{12}
Sn3	0.0158(4)	0.0120(3)	0.0131(3)	0.0011(2)	–	–
$Rb_8Hg_4Sn_{42}$ (**2**)						
Rb1	0.0222(7)	U_{11}	U_{11}	–	–	–
Rb2	0.040(1)	0.089(1)	U_{22}	–	–	–
Hg/Sn1	0.0198(4)	0.0298(5)	U_{11}	–	–	–
Sn2	0.0148(2)	U_{11}	U_{11}	–0.0009(1)	U_{12}	U_{12}
Sn3	0.0170(3)	0.0143(3)	0.0150(3)	0.0006(2)	–	–
$Cs_8Hg_4Sn_{42}$ (**3**)						
Cs1	0.0173(4)	U_{11}	U_{11}	–	–	–
Cs2	0.0281(8)	0.0554(6)	U_{22}	–	–	–
Hg/Sn1	0.0198(3)	0.0285(5)	U_{11}	–	–	–
Sn2	0.0147(2)	U_{11}	U_{11}	–0.0009(1)	U_{12}	U_{12}
Sn3	0.0168(3)	0.0152(3)	0.0146(3)	0.0007(2)	–	–

Interestingly, the size of the cation does not only drastically affect the rattling effects but also correlates with the thermal stability of the clathrates. According to differential thermal analysis (DTA) each compound shows upon heating one major endothermic transition with large thermal hysteresis, which is assigned to incongruent melting. In order to compare the thermal stabilities of the binary[12] and Hg-substituted clathrates, we also synthesized the binary compounds $A_8Sn_{44}\square_2$ for A = K, Rb[8a] and Cs.[8b] For both series, melting points increase with increasing atomic number of the alkali metals, and in all cases, the Hg-substituted clathrates appear to be thermally more stable than the corresponding defect clathrates (Table 4). Finally, the DTA diagrams of the Hg-substituted clathrates show a weak reversible transition at about 195 °C, which confirms the existence of a Hg_xSn_{10-x} phase[13] ($x \approx 1$); β-Sn, which melts at 232 °C, was not observed.

The X-ray powder diagrams of the reaction products confirm that compounds **1**–**3** contain small amounts of the binary phase Hg_1Sn_9 as an impurity. Rietveld analysis of **3** shows a content of Hg_1Sn_9 admixture [space group *P6/mmm*, a = 3.20863(8) Å and c = 2.98648(8) Å] of 5.2(1)% (Figure 2). A SQUID measurement was carried out for **3** showing temperature-independent diamagnetic behavior (χ = –5.5 10^{-4} emu mol^{-1}), as expected for an electron-precise Zintl phase. The increase in the magnetic susceptibility at very low temperatures is assigned to paramagnetic Hg_1Sn_9. Most probably, this is also the cause of the superconducting magnetic transition at about 4 K (T_c = 3.7 K for β-Sn and T_c = 4.1 K for Hg), when the magnetization was measured at low field (0.01 Tesla).

Table 4. Onsets of the melting for the $A_8Sn_{44}\square_2$ and $A_8Hg_4Sn_{42}$ clathrate compounds.

Compound	Temperature / °C
$K_8Sn_{44}\square_2$	395
$K_8Hg_4Sn_{42}$	446
$Rb_8Sn_{44}\square_2$	511
$Rb_8Hg_4Sn_{42}$	548
$Cs_8Sn_{44}\square_2$	577
$Cs_8Hg_4Sn_{42}$	627

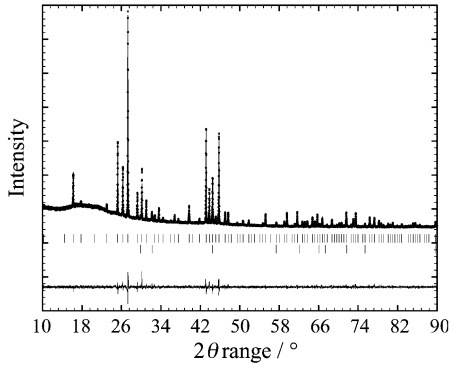

Figure 2. X-ray powder diagram (○) and theoretical pattern (solid line) for the $Cs_8Hg_4Sn_{42}$ sample. The top and bottom rows of vertical lines represent the Bragg reflections of $Cs_8Hg_4Sn_{42}$ and Hg_1Sn_9, respectively. Also shown below is the difference between the observed and the theoretical pattern.

Once again, the question regarding the exact composition of the clathrates arises. Initially, the occupation factors for the Hg/Sn1 positions were set free in the single-crystal refinements. This led to the corresponding values 0.66/0.34(1), 0.607/0.393(9), and 0.61/0.39(1) for **1**, **2** and **3**, respectively, which resulted in the compositions $K_8Hg_{3.94(6)}Sn_{42.06(6)}$, $Rb_8Hg_{3.64(6)}Sn_{42.36(6)}$, and $Cs_8Hg_{3.67(6)}Sn_{42.33(6)}$. Thus, within standard deviation (3σ range) the same composition results, and by considering correlation effects between ADPs and the site occupation parameters even larger standard deviations must be assumed. Our EDX analyses confirm the presence of A, Sn and Hg in the expected ratio; however, the accuracy is lower than the crystallographically determined one. Several X-ray data refinements of different crystals of the same compound obtained from other stoichiometries used for the syntheses (A/Hg/Sn = 8:6:40) always resulted in the same composition of the main product with deviations in the occupancy parameters of less than 0.03(3).

As a result of the diamagnetic behaviour of **3** and the absence of a phase width, the Hg/Sn1 ratio was constrained to 0.667:0.333 or the composition $A_8Hg_4Sn_{42}$. A neutral framework of 46 tin atoms per unit cell with exclusive cova-

lently four-bonded Sn atoms requires $46 \times 4 = 184$ valence electrons. In $A_8Hg_4Sn_{42}$, 42 Sn atoms provide 168 electrons and 4 Hg atoms $4 \times 2 = 8$ electrons. By applying the Zintl–Klemm concept, an additional 8 electrons are contributed to framework bonding by the 8 alkali-metal atoms, which overall results in 184 valence electrons. Therefore, the title compounds are electron-precise Zintl phases. In contrast, our current results on isostructural A–Hg–Ge clathrates show significantly lower Hg content and metallic character.[14]

Conclusions

In these first examples of Hg-substituted clathrates, mercury follows the trends of its lighter homologues, namely, M = Zn, Cd in $Cs_8M_4Sn_{42}$.[9,15] Despite the rather unusual tetrahedral coordination, it forms stable bonds with the Sn atoms, as indicated by comparing the thermal stability of $A_8Sn_{44}\square_2$ and $A_8Hg_4Sn_{42}$, where A = K, Rb or Cs. The encapsulation of larger alkali metals avoids strong rattling in the cavities and enhances the overall stability. This rationalises the fact that no type-I Sn clathrates with encaged small cations such as Na^+, Cu^+ and Ag^+ have been synthesized so far. Finally, the title compounds are the heaviest members of the rapidly increasing family of semiconducting clathrates doped with group 11–13 elements.[16] Therefore, they also appear particularly interesting for minimizing the lattice thermal conductivity.

Experimental Section

Synthesis: The starting materials used for the synthesis were stored in an Ar-filled glove box: K (Merck, 99%), Rb (Riedel de Haën, 99.9%), Cs (Riedel de Haën, 98%+), Hg (Aldrich, 99.99%+) and Sn (Chempur, granules, 99.999%). Stoichiometric mixtures of the reagents (1.0–1.5 g) were loaded in niobium ampoules. The ampoules were then sealed by welding and enclosed in quartz tubes. The samples were heated at a rate of 2 °C min^{-1} to 650 °C and held at the temperature for 24 h, annealed at 400 °C (for **1**) or 450 °C (for **2** and **3**) for 10 d and subsequently cooled down to room temperature at a rate of –3 °C min^{-1}. Air-stable, metal-like crystals of the corresponding clathrates were extracted from the reaction mixtures.

X-ray Powder Diffraction: The phase analysis of the products was carried out by X-ray powder diffraction with a STOE STADI P2 diffractometer [Ge(111) monochromator for Cu-K_α radiation: λ = 1.54056 Å] equipped with a linear position sensitive detector ($2\theta_{eff}$ ca. 40°). The crystals were finely ground in an agate mortar to a homogeneous powder and were measured in transmission mode. The patterns were refined with the Rietveld method.[17]

Single-Crystal X-ray Diffraction: Good-quality single crystals of compounds **1**, **2** and **3** were mounted on an Oxford Xcalibur3 diffractometer for full data collection at room temperature (CCD detector, graphite monochromator for Mo-K_α radiation: λ = 0.71073 Å). Three series of 138 frames were recorded with exposure times of 30 s and a crystal-detector distance of 50 mm. The reflections were collected over the range $2\theta_{max}$ = 50.5° and corrected for absorption (multi scan) by using the program CrysAlis RED (Oxford Diffraction Ltd). Systematic absence conditions were consistent with the space group $Pm\bar{3}n$ (Nr. 223). The data were processed by using the SHELXTL package.[18] The structures were successfully solved by direct methods and yielded satisfactory residuals. Relevant crystallographic and refinement data are listed in Table 5. Further details of the crystal-structure investigations may be obtained from the Fachinformationszentrum Karlsruhe, 76344 Eggenstein-Leopoldshafen, Germany, on quoting the depository numbers CSD-417501 (for **1**), -418008 (for **2**) and -418007 (for **3**).

Thermal Analysis: The thermal stability of the products was investigated by differential thermal analysis (NETZSCH 404C). The samples (about 300 mg each) were loaded and weld shut in Nb crucibles and then heated under a continuous argon flow from room temperature at the rate of 5 °C min^{-1} to 1000 °C and cooled down at the same rate. Two successive loops were run for each sample.

Magnetic Measurements: The measurements for **3** were performed with a SQUID magnetometer (Quantum Design MPMS XL-5). The polycrystalline sample (34.4 mg) was first zero-field cooled to 2 K and checked for superconductivity at a field of 0.01 Tesla. The temperature-independent susceptibility of –5.5 10^{-4} emu mol^{-1} was obtained by measuring the powdered sample in the temperature range 2–400 K at a field of 2 Tesla. Small contributions to the

Table 5. Crystallographic data and refinement parameters for Hg-substituted clathrates **1**, **2** and **3**.

Empirical formula	$K_8Hg_4Sn_{42}$	$Rb_8Hg_4Sn_{42}$	$Cs_8Hg_4Sn_{42}$
Formula weight	6100.14	6471.10	6850.62
Space group	$Pm\bar{3}n$	$Pm\bar{3}n$	$Pm\bar{3}n$
Z	1	1	1
Unit cell parameter, a /Å	12.1255(4)	12.1838(4)	12.2130(4)
Unit cell volume, V /Å^3	1782.8(1)	1808.6(1)	1821.7(1)
$\rho_{calcd.}$ /g cm^{-3}	5.682	5.941	6.245
Absorption coeff., μ /mm^{-1}	23.436	27.989	26.419
F (000)	2572	2716	2860
θ range /°	3.36–25.39	3.34–25.26	3.34–25.19
No. of integrated reflections	10422	10588	10592
No. of independent reflections	323 (R_{int} = 0.064)	323 (R_{int} = 0.032)	323 (R_{int} = 0.031)
No. of parameters	16	16	16
Goodness-of-fit on F^2	1.337	1.178	1.339
Final R indices[a]	R_1 = 0.019, wR_2 = 0.051	R_1 = 0.017, wR_2 = 0.043	R_1 = 0.017, wR_2 = 0.038
Final R indices (all data)	R_1 = 0.020, wR_2 = 0.051	R_1 = 0.018, wR_2 = 0.044	R_1 = 0.018, wR_2 = 0.039
Residual map /e Å^{-3}	0.76/–0.83	0.63/–1.32	0.64/–0.94

[a] Final weighting scheme = $1/[\sigma^2(F_o^2)+(0.0217P)^2 + 12.63P]$ for **1**, $1/[\sigma^2(F_o^2) + (0.0190P)^2 + 19.46P]$ for **2** and $1/[\sigma^2(F_o^2) + (0.0110P)^2 + 19.04P]$ for **3**, where $P = (F_o^2 + 2F_c^2)/3$.

susceptibility from the Hg_xSn_{10-x} ($x \approx 1$) impurity were extrapolated from comparable amounts of β-Sn and found to be negligible.

EDX Analyses: These were carried out for single crystals with a JEOL 5900LV scanning electron microscope system operating at 20 kV and equipped with a LINK AN 10000 detector system.

Acknowledgments

This work is supported by the European Union within the RTN program (EU-project Nr. HPRN-CT 2002–00193).

[1] a) F. J. DiSalvo, *Science* **1999**, *285*, 703–706; b) G. S. Nolas, J. Poon, M. Kanatzidis, *MRS Bull.* **2006**, *31*, 199–205.
[2] B. Iversen, A. E. C. Palmqvist, D. E. Cox, G. S. Nolas, G. D. Stucky, N. P. Blake, H. Metiu, *J. Solid State Chem.* **2000**, *149*, 455–458.
[3] G. Slack, *CRC Handbook of Thermoelectrics,* CRC Press, **1995**.
[4] a) G. S. Nolas, J. L. Cohn, G. A. Slack, S. B. Schujman, *Appl. Phys. Lett.* **1998**, *73*, 178–180; b) J. L. Cohn, G. S. Nolas, V. Fessatidis, T. H. Metcalf, G. A. Slack, *Phys. Rev. Lett.* **1999**, *82*, 779–782; c) N. P. Blake, L. Mollnitz, G. Kresse, H. Metiu, *J. Chem. Phys.* **1999**, *111*, 3133–3144.
[5] a) M. A. Avila, D. Huo, T. Sakata, K. Suekuni, T. Takabatake, *J. Phys.: Condens. Matter.* **2006**, *18*, 1585–1592; b) M. Christensen, N. Lock, J. Overgaard, B. B. Iversen, *J. Am. Chem. Soc.* **2006**, *128*, 15657–15665.
[6] a) G. S. Nolas, B. C. Chakoumakos, B. Mahieu, G. J. Long, T. J. R. Weakley, *Chem. Mater.* **2000**, *12*, 1947–1953; b) S. Paschen, M. Baenitz, V. H. Tran, A. Rabis, F. Steglich, W. Carrillo-Cabrera, Yu. Grin, A. M. Strydom, P. de V. du Plessis, *J. Phys. Chem. Solids* **2002**, *63*, 1183–1188; c) J. V. Zaikina, W. Schnelle, K. A. Kovnir, A. V. Olenev, Yu. Grin, A. V. Shevelkov, *Solid State Sci.* **2007**, *9*, 664–671.
[7] G. C. Che, M. Ellner, K. Schubert, *J. Mater. Sci.* **1991**, *26*, 2417–2420.
[8] a) F. Dubois, T. Fässler, *J. Am. Chem. Soc.* **2005**, *127*, 3264–3265; b) A. Kaltzoglou, S. D. Hoffmann, T. F. Fässler, *Eur. J. Inorg. Chem.* **2007**, 4162–4167.
[9] G. Nolas, T. Weakley, J. L. Cohn, *Chem. Mater.* **1999**, *11*, 2470–2473.
[10] F. Merlo, M. Pani, M. L. Fornasini, *J. Alloys Compd.* **1993**, *196*, 145–148.
[11] M. Lutz, B. Findeis, M. Haukka, R. Graff, T. A. Pakkanen, L. H. Gade, *Chem. Eur. J.* **2002**, *8*, 3269–3276.
[12] a) M. Baitinger, PhD Thesis, Technical University Darmstadt, **2000**; b) H.-G. von Schnering, R. Kröner, M. Baitinger, K. Peters, R. Nesper, Yu. Grin, *Z. Kristallogr. - New Cryst. Struct.* **2000**, *215*, 205–206.
[13] T. B. Massalski, H. Okamoto, P. R. Subramanian, L. Kacprzak, *Binary Alloy Phase Diagrams* 5th ed., ASM-International, Materials-Park, **2004**.
[14] a) S. Ponou, PhD Thesis, Technische Universität München, **2006**; b) S. Ponou, A. Kaltzoglou, T. F. Fässler, manuscript in preparation.
[15] A. P. Wilkinson, C. Lind, R. A. Young, S. D. Shastri, P. L. Lee, G. S. Nolas, *Chem. Mater.* **2002**, *14*, 1300–1305.
[16] K. A. Kovnir, A. V. Shevelkov, *Russ. Chem. Rev.* **2004**, *73*, 923–938.
[17] T. Roisnel, J. Rodriguez-Carvajal, *FULLPROF*, version 3.20 LLB-LCSIM, March **2005**, France.
[18] *SHELXTL*, Bruker Analytical X-ray Instruments, Madison, WI, **1998**.

Received: August 16, 2007
Published Online: November 28, 2007

